AIAA 92-0462

Primary Breakup in Gas/Liquid Mixing Layers for Turbulent Liquids

P.-K. Wu, L.-K Tseng and G. M. Faeth
University of Michigan
Ann Arbor, MI

30th Aerospace Sciences Meeting & Exhibit
January *6-9/1992* / Reno, NV

AIAA-92-0462

PRIMARY BREAKUP IN GAS/LIQUID MIXING LAYERS FOR TURBULENT LIQUIDS§

P.-K. Wu,* L.-K. Tseng** and G.M. Faeth†
Department of Aerospace Engineering
The University of Michigan, Ann Arbor, Michigan 48109-2140

Abstract

An experimental study of primary breakup of turbulent liquids in gas/liquid mixing layers is described. The experiments involved mixing layers along large liquid jets (3.6, 6.4 and 9.5 mm dia.) injected at various velocities into still air at atmospheric pressure with fully-developed turbulent pipe flow at the jet exit. Liquids studied included water, glycerol (42% glycerin by mass) and n-heptane. Pulsed shadowgraph photography and holography were used to find conditions where turbulent primary breakup was initiated and drop sizes and velocities after primary breakup. Drop sizes after primary breakup satisfied Simmons' universal root normal distribution and can be characterized solely by their SMD. Mass weighted mean streamwise and crosstream drop velocities after primary breakup were comparable to mean streamwise and crosstream rms fluctuating velocities in the liquid, respectively, with effects of mean velocity distributions in the jet passage reflected by somewhat lower streamwise drop velocities near the jet exit. Conditions for the initiation of turbulent primary breakup and the variation of SMD with distance from the jet exit were correlated reasonably well by a phenomenological analyses considering effects of surface tension and liquid turbulence properties alone. However, limited data in the literature indicates that aerodynamic effects begin to influence drop sizes after primary breakup at ambient pressures greater than atmospheric pressure.

Nomenclature

C_{si}	= empirical constant for SMD at onset of breakup
C_{sx}	= empirical constant for SMD variation with x
C_{xi}	= empirical constant for x at onset of breakup
d	= injector diameter
d_{max}, d_{min}	= maximum and minimum image dimensions of drops
d_p	= drop diameter
e_p	= volume-averaged ellipticity
ℓ	= characteristic eddy size
ℓ_k	= Kolmogorov length scale
L_c	= liquid core length
L	= Rayleigh breakup length
MMD	= mass median diameter
	= Ohnesorge number, $\mu_f / (\rho_f d\sigma)^{1/2}$
Re_{fd}	= jet Reynolds number, $\bar{u}_o d/\nu_f$
SMD	= Sauter mean diameter
u	= streamwise velocity
u_p	= streamwise drop velocity
v	= radial velocity
v_ℓ	= radial velocity associated with eddy of size ℓ
v_p	= radial drop velocity
We_{ij}	= Weber number based on phase i and length scale j, $\rho_i \bar{u}_o^2 j/\sigma$
x	= streamwise distance
A	= radial integral length scale
μ	= molecular viscosity
ν	= kinematic viscosity
ρ	= density
σ	= surface tension
τ	= characteristic drop formation time

Subscripts

f	= liquid-phase property
g	= gas-phase property
i	= at point of breakup initiation
o	= jet exit condition

Superscripts

$\bar{()}$	= time-averaged mean properties
$\tilde{()}$	= mass-averaged mean property
$()'$	= time-averaged rms fluctuating property

Introduction

Primary breakup to form drops near liquid surfaces is an important fundamental process with applications to liquid atomization, gas injection into liquids and multiphase flow in tubes, among others. Primary breakup is important because it determines the initial properties of the dispersed phase which affects mixing rates, secondary breakup, collisions and separated flow within the dispersed flow region. Motivated by these considerations, an experimental study of primary breakup of nonturbulent liquids in gas/liquid mixing layers recently was completed in this laboratory.[1] The objective of the present investigation was to extend this work to consider primary breakup of turbulent liquids because this condition is encountered in practice as well. Similar to Ref. 1, measurements were carried out within the gas/liquid mixing layer at the periphery of round liquid jets in still air. This region corresponds to the near-injector dense-spray region of a pressure-atomized spray for atomization breakup conditions.

Past studies of pressure-atomized sprays have established that spray properties are influenced by turbulence at the jet exit. First of all, the early studies of pressure atomization by De Juhasz et al.[2] and Lee and Spencer3 showed that both atomization quality and mixing rates differed for laminar and turbulent flow at the jet exit. Next, Grant and Middleman4 and Phinney[5] observed that jet stability and the onset of breakup were affected by turbulence at the jet exit as well. Finally, Hiroyasu et al.6 and Chehroudi et al.7 studied the length of the all-liquid core near the jet exit, which resembles the potential core region of single-phase jets. Their results suggest that the length of the liquid core is affected by turbulence at the jet exit,

---

* Graduate Assistant, Department of Aerospace Engineering, The University of Michigan, Ann Arbor, Michigan 48109-2140.

** Research Fellow, Department of Aerospace Engineering, The University of Michigan, Ann Arbor, Michigan 48109-2140.

† Professor, Department of Aerospace Engineering, The University of Michigan, Ann Arbor, Michigan 48109-2140.

somewhat analogous to the effect of jet exit turbulence on the length of the potential core of single-phase jets.

Work in this laboratory by Ruff et al.[8-10] and Tseng et al.[11,12] has helped to quantify effects of turbulence at the jet exit on mixing rates and structure of the dispersed-phase region of pressure-atomized sprays. These experiments involved relatively large round water jets (9.5 and 19.1 mm dia.) in still air at ambient pressures of 1-8 atm, with both nonturbulent slug flow and fully-developed turbulent pipe flow at the jet exit. These experiments emphasized atomization breakup conditions, where drops begin to form right at the jet exit and the liquid core is completely surrounded by the dispersed-flow region. This was done because the atomization breakup regime dominates most practical applications due to the small range of liquid flow rates and poor atomization qualities of the other breakup regimes.8

The measurements of Ruff et al.[8-10] and Tseng et al.[11,12] involved mean liquid volume fraction distributions using gamma-ray absorption and dispersed-phase properties using pulsed holography. The measurements of liquid volume fraction distributions showed much faster mixing rates for fully-developed turbulent pipe flow than for nonturbulent slug flow at the jet exit.[8,11] Observed effects of jet exit turbulence on mean liquid volume fraction distributions were predicted reasonably well (for mean liquid volume fractions greater than 0.2) using the locally homogeneous flow (LHF) approximation, where interphase transport rates are assumed to be infinitely fast, i.e., relative velocities between the phases are ignored. This suggests significant effects of liquid turbulence on primary breakup because it represents the first stage of mixing. The pulsed holography measurements of drop sizes confirmed the effects of liquid turbulence on primary breakup.[9,10,12] In general, drop sizes after primary breakup were larger for turbulent than nonturbulent liquids, approaching the dimensions of spatial integral scales in the liquid for turbulent primary breakup. Additionally, relative velocities between the phases were large near the liquid surface, implying significant effects of separated flow in the dispersed-flow region. It was inferred that liquid turbulence properties dominated the outcome of turbulent primary breakup at atmospheric pressure, with aerodynamic effects becoming more important at elevated pressures and causing drop sizes after primary breakup to become smaller.[9,10,12] However, the mechanism of turbulent primary breakup was not pursued in any detail in these studies due to the relatively limited data base on drop properties near the liquid surface (water jets having only one jet exit velocity).

The previous review of the literature shows that past work has established significant differences between nonturbulent and turbulent primary breakup and has demonstrated that turbulent primary breakup enhances the mixing rates of pressure-atomized sprays. However, existing information about turbulent primary breakup is limited and the mechanism is not understood. In particular, no methods are available to estimate either the conditions for the onset or the subsequent outcome of turbulent primary breakup which impedes consideration of separated flow phenomena in the dispersed flow region.

In order to help fill this gap in the literature, the objectives of the present investigation were to observe the onset and outcome of turbulent primary breakup for a wide range of test conditions, and to use the measurements, as well as results available from Refs. 9,10 and 12, to develop approximate theories of these processes. Present experiments involved relatively large round liquid jets (3.6, and 6.4 mm dia.) in still air at atmospheric pressure with fully-developed turbulent pipe flow at the jet exit. Effects of flow dynamics and liquid physical properties were studied by considering various jet exit velocities and liquids (water, 42% glycerol and n-heptane). Measurements included pulsed shadowgraph photography and holography to find conditions for the onset of turbulent primary breakup as well as drop sizes and velocities produced by this breakup mechanism.

The paper begins with a description of experimental methods. Results are then considered treating flow visualization, drop size distributions, drop velocities, onset of breakup and drop sizes and shapes, in turn. The paper concludes with discussion of potential aerodynamic effects on turbulent primary breakup, based on recent measurements at elevated ambient pressures due to Tseng et al.[12]

Experimental Methods

Apparatus

The following description of experimental methods will be brief because they are similar to the earlier study of nonturbulent primary breakup.[1] The apparatus consists of a pneumatically driven piston/cylinder arrangement containing the liquid to be injected with the liquid outlet centered on the axis of the piston. The piston has a diameter of 64 mm and a stroke of 200 mm, yielding a liquid sample size of roughly 600 ml. The outlet of the cylinder was rounded to prevent cavitation and was followed by a constant diameter passage having a length to diameter ratio of 41, to yield nearly fully developed turbulent pipe flow at the jet exit, similar to Ruff et al.[8] Jet passage diameters considered during the tests were 3.6 and 6.4 mm. Injection was vertically downward with the liquid collected in a baffled tub and then discarded. Instrumentation was mounted rigidly; therefore, various positions in the flow were studied by traversing the entire injector assembly.

The piston/cylinder arrangement was filled with the test liquid while venting trapped air from just below the piston face. Operation was initiated by admitting high-pressure air to the upper side of the piston through a solenoid valve which forced the liquid through the jet passage. Total times of injection were 180-1400 ms due to the definite liquid sample size. These relatively short time periods were not problematical, however, because flow development times are generally less than 1% of the flow time for the near-injector region where measurements were made while pulsed photography and holography only required times in the range 1-32 μs for triggering and data accumulation. Jet exit velocities at the time of the measurements were calibrated using an impact plate as described in Ref. 1.

Instrumentation

Photography. Pulsed shadowgraph photography was used to measure properties at the onset of turbulent breakup, where relatively low dispersed-phased concentrations makes this approach feasible and convenient. The holocamera was used for this purpose, operating in the single-pulse mode with the reference beam blocked to yield a shadowgraph rather than a

hologram. The optics were arranged to give a primary magnification of 3:1 on the film. Drops were sized using an image analysis system in the same manner as the holography measurements to be discussed next. These photographs also were used to find the streamwise location of the onset of turbulent primary breakup. Experimental uncertainties (95% confidence) of this determination were generally less than 40%, the relatively large value being due to innate statistical variations of this event, i.e., whether drops completely detached from ligaments at the time the photograph was obtained.

Holography. The double-pulse holocamera and reconstruction systems were similar to the arrangements used by Ruff et al.[9,10] Present optics provided a 5-6:1 magnification of the hologram image itself, coupled with reconstruction optics that allowed measurements of drop diameters as small as 5 μm. The laser could be double pulsed with pulse separation times as short as 1 μs, to accommodate measurements of both large streamwise and small crosstream velocities of drops. The properties of the reconstructed sprays were analyzed using a Gould FD 5000 image display system with a field of view of 1.4 x 1.6 mm. Various locations in the hologram reconstructions could be observed by traversing the hologram in two directions and the video camera of the display system in the third direction.

Drops and other ellipsoidal objects were sized by measuring their maximum and minimum diameters through the centroid of the image. Assuming ellipsoidal shapes, the diameter of these objects was taken to be the diameter of a sphere having the same volume, $d_p^3 = d_{min}^2 d_{max}$. The shape of the object was described by its ellipticity, defined as $e_p = d_{max} / d_{min}$. More irregular objects were sized by finding the area and perimeter of their image, and computing the maximum and minimum diameters of an ellipsoid matching these properties: given these parameters, d_p and e_p were found as before. Results at each condition were summed, considering 20-400 elements, to provide drop size distributions, mass median diameter (MMD), Sauter mean diameter (SMD) and the volume averaged ellipticity, e_p. Experimental uncertainties were generally dominated by finite sampling limitations because there are relatively few drops after turbulent primary breakup due to relatively large drop sizes. Within the limitations of definitions of liquid element sizes and ellipticities, which are difficult to quantify, estimated experimental uncertainties (95% confidence) are estimated to be less than 38% for MMD and SMD and 39% for e_p.

Drop velocity measurements were based on the motion of the centroid of the image, allowing streamwise and crosstream velocities to be computed from the known intervals between laser pulses. Directional ambiguity was resolved by using different light intensities for the two laser pulses because the larger pulse yielded a sharper image of the drops. Results at each condition were summed, considering 20-400 elements, to obtain mass-weighted (Favre) averaged drop velocities. Experimental uncertainties were dominated by finite sampling limitations, with the accuracy of finding the centroid of large irregular liquid elements also being a factor for the relatively small radial velocities that were observed. The resulting experimental uncertainties (95% confidence) are estimated to be less than 19% for $\tilde{u}_p$ and less than 60% for the much smaller values of $\tilde{v}_p$.

Test Conditions

Test conditions are summarized in Table 1. A series of holograms for the region along the liquid surface were available from Ruff et al.[9,10] and Tseng et al.[12], and were used to provide results for water for a jet exit diameter of 9.5 mm at atmospheric pressure. The remainder of the measurements were obtained using the present apparatus with jet exit diameters of 3.6 and 6.4 mm. All injectors involved fully-developed turbulent pipe flow at the jet exit with passage length-to-diameter ratios of 41. In particular, Ruff et al.[8] measured flow properties at the exit of the 9.5 mm passage, finding distributions of mean and rms fluctuating velocities in agreement with results in the literature for the corresponding range of Reynolds numbers[13,14], within experimental uncertainties. In view of this, streamwise and radial integral integral length scales of the flow at the jet exit were taken to be 0.4d and d/8, respectively, based on measurements of Laufer for fully developed turbulent pipe flow cited in Hinze.[14]

The streamwise positions of present measurements involved x/d in the range 0.2-100. Earlier work,[4,6,7] indicates that the length of the liquid core was in excess of x/d = 200 for present test conditions. Thus, present measurements involve breakup at the surface of the liquid core rather than breakup of the entire liquid column itself

Test liquids included water, a glycerin/water mixture (42% glycerin, by mass) and n-heptane. This provided the following ranges of fluid properties: liquid/gas density ratios of 575-927, liquid viscosities of $3.94\text{-}34.66 \times 10^{-4}$ kg/ms and surface tensions of $2.00\text{-}7.08 \times 10^{-2}$ N/m^2. These fluid properties were verified as described in Ref. 1.

Jet exit velocities were in the range 16-109 m/s, yielding jet dynamic parameters as follows: Re_{fd} of 110,000-780,000, We_{gd} of 27-1257, We_{fd} of 2.3-109 and Oh_d of 0.0011-0.0024. Most test conditions involved $We_{fd} > 8$ and $We_{gd} > 40.3$ which places them in the atomization breakup regime where breakup should begin right at the jet exit according to jet breakup criteria for nonturbulent liquids due to Miesse[15] and Ranz.[16] A few test conditions for water were in the wind-induced breakup regime, where breakup begins along the sides of the liquid jet at some distance from the jet exit, according to the criteria of Refs. 15 and 16. Actually, the first appearance of drops from turbulent primary breakup is only crudely described by the criteria of Refs. 15 and 16 and always occurred at some distance from the jet exit: this will be discussed later in more detail.

Results and Discussion

Flow Visualization

Consideration of the results will begin with visualization of the flow in order to provide insight concerning the general nature of the turbulent primary breakup process. Shadowgraphs of the flow near the liquid surface at various distances from the jet exit are illustrated in Fig. 1. These results are for water with d = 3.6 mm, with the relatively small injector diameter helping to minimize obscuration problems of the shadowgraph technique. The direction of motion of the liquid in the photographs is vertically downward, which corresponds to the orientation of the experiment. Three photographs are shown : one right at the jet exit (which can be seen at the top of this photograph) in the region of initiation of breakup, and the other two centered at x/d

= 10 and 50, respectively. A 0.9 mm diameter pin is visible in the latter two photographs to provide a size and distance reference. The liquid core is to the left in all three photographs.

The photographs of Fig. 1 illustrate a number of general features of the liquid surface during turbulent primary breakup. First of all, even though the test condition is well within the atomization breakup regime defined by Refs. 15 and 16 (e.g., $We_{gd} = 72$), where breakup should begin right at the jet exit, the surface just becomes roughened or distorted very close to the jet exit while the first appearance of drops is deferred to x/d of roughly 0.3. A second feature of the liquid surface is that its mean position bulges outward within the first few diameters in the streamwise direction. Predictions based on the LHF approximation suggest that this is due to evolution of the mean velocity profile in the liquid from turbulent pipe flow conditions to a nearly flat profile consistent with the relatively low effects of drag on the liquid surface from the gas.[8,11] Another property of the liquid surface is that the scale of surface distortions progressively increases with increasing distance from the jet exit, in fact, small scale distortions are not even superimposed on the large wave-like structures seen at x/d = 50. Similar behavior was observed by Ruff et al.[8] for turbulent liquid jets in the first wind-induced breakup regime in the region prior to the onset of breakup; in particular, the liquid surface exhibited fine-grained roughness near the jet exit, with the surface becoming smoother with larger-scale irregularities appearing as the distance from the jet exit increased. This behavior can be attributed to two effects. First of all, small disturbances complete their growth more rapidly than large disturbances (as discussed later) so that they should appear first. The second effect involves reduced levels of turbulence production as mean velocities become more uniform in the liquid. This causes the turbulence to decay with increasing distance from the jet exit, with the small-scale high wave number range of the turbulence spectrum disappearing first, tending to reduce fine-grained distortion of the liquid surface accordingly. It seems likely that similar processes continue to act even in the presence of primary breakup yielding the properties of turbulent distortion of the liquid surface seen in Fig. 1. Finally, the ligament-like structures protruding from the liquid surface exhibit little effect of drag from the gas phase — being randomly oriented from the liquid surface rather than predominantly deflected backward toward the jet exit due to drag from the more slowly moving gas.[19] This suggests that the primary breakup process is dominated by the properties of the liquid turbulence rather than aerodynamic stripping for present test conditions. Such behavior is not surprising in view of the relatively large size of the ligaments and their relatively short residence times protruding into the flow: consideration of velocity relaxation times for drops of comparable size[9,10] indicates that the ligaments do not appreciably accommodate to global gas velocities in the period while they are attached to the surface.

Turning to drop properties seen in Fig. 1, it is evident that drop diameters near the liquid surface progressively increase with distance from the jet exit, similar to the scale of surface distortions. Additionally, examination of the surface distortion of individual ligaments, as well as drops apparently associated with some ligaments, suggests that separation of drops from attached ligaments occurs by a process analogous to Rayleigh breakup, i.e., the ligaments act somewhat like liquid jets in the Rayleigh breakup regime. Some of the larger ligament-like drops in the flow appear to be undergoing additional division by Rayleigh breakup as well. Other features of the flow are similar to earlier observations of the dispersed flow region for turbulent primary breakup conditions:[9,10,12] the region of the liquid surface has the largest and most irregular drops with smaller round drops near the edge of the flow, suggesting significant effects of secondary breakup; drop number densities increase with increasing distance from the jet exit but liquid volume fractions remain surprisingly low, tending to minimize potential effects of collisions; and the width of the dispersed flow region progressively increases with increasing distance from the jet exit because drops have more residence time to move away from the surface due to their initial radial velocities after breakup and effects of turbulent dispersion.

Hologram reconstructions of the flow near the liquid surface for various liquid velocities at a fixed distance from the jet exit are illustrated in Fig. 2. These results are for water at x/d = 10 with d = 6.4 mm. The direction of motion on the photographs is vertically downward and the 0.9 mm diameter reference pin is present as before, however, this time the liquid core is to the left of the photographs. Conditions at three liquid velocities are shown: 22, 40 and 81 m/s.

Significant effects of liquid velocity on the distortion of the liquid surface can be seen in the photographs of Fig. 2. First of all, while the size of the larger scale disturbances are similar for all three velocities (a property that was more evident by observing larger sections of the surface than shown in Fig. 2), the smallest scale disturbances become progressively smaller as the liquid velocity increases. This behavior also is similar to the distortion of the surface of turbulent liquid jets before primary breakup begins, where large scale features are not strongly affected by the jet Reynolds number but increasing Reynolds numbers increases the degree of fine-grained surface roughness.[8] This appears to be an effect of the power spectrum of the liquid turbulence, where the kinetic energy available to distort the surface at high wave numbers increases as the Reynolds number (which is proportional to the liquid velocity for the conditions of Fig. 2) increases. In a sense, this process is the inverse of the effect of distance from the jet exit seen in Fig. 1, where decay of the turbulence affects the high wave numbers first, tending to reduce the degree of fine-grained distortion of the surface with increasing distance from the jet exit. Finally, the direction of the ligaments protruding from the surface is not particularly correlated with the relative velocity of the gas, even at the highest relative velocity. This suggests that the motion of the ligaments is largely the result of randomly directed liquid velocity fluctuations, with aerodynamic drag forces playing a secondary role for present test conditions.

Similar to Fig. 1, drop properties after primary breakup in Fig. 2 generally are related to the properties of the distortion of the liquid surface. Thus, drop sizes tend to decrease, similar to the reduction of the size of surface disturbances or attached ligaments, as the liquid velocity increases. It is also seen that the number density of drops near the liquid surface increases as the relative velocity increases. This mainly is caused by the reduction of drop sizes with increasing relative velocities because liquid volume fractions in the dispersed phase are relatively independent of flow conditions for the high jet Reynolds numbers of present tests.[8,9,11,12]

Drop Size Distributions

Drop size distributions after turbulent primary breakup were measured locally for all present test conditions. It was found that the size distribution functions agreed with Simmons'[17] universal root normal distribution function with the ratio MMD/SMD = 1.17 and the 95% confidence interval for this ratio being 1.11-1.23. This behavior agrees with earlier measurements of drop size distributions in sprays which find MMD/SMD = 1.20 with similar 95% confidence intervals: Ruff et al.[10] and Tseng et al.[12] for conditions along the liquid surface and throughout the dispersed flow region for pressure atomized sprays with both nonturbulent and turbulent jet exit conditions, Wu et al.[1] after primary breakup of nonturbulent liquids, and the original recommendation of Simmons[17] based on observations of industrial sprays. Since the root normal distribution only has two moments, the best estimate of MMD/SMD = 1.2 implies that the entire drop size distribution is known if the SMD is known. Thus, drop sizes will be described in terms of SMD alone in the following.

Drop Velocities

Drop velocities after primary breakup will be considered next, in order to help define the dynamic properties of the primary breakup. Available measurements of volume (mass) averaged streamwise and crosstream drop velocities, both normalized by $\bar{u}_o$, are plotted as a function of x/d in Fig. 3. The measurements include all the test liquids and jet diameters at various jet exit velocities, drawing results for d = 9.5 mm from Ruff et al.[9]

The normalized drop velocities for all test conditions illustrated in Fig. 2 generally correlate as functions of x/d, with the larger scatter for $\tilde{v}_p/\bar{u}_o$ being consistent with earlier estimates of the larger experimental uncertainties of this velocity component due to its relatively small magnitude. Very near the jet exit, $\tilde{u}_p/\bar{u}_o$ has a value of roughly 0.6 which increases to reach a value near unity for x/d > 20. This behavior can be explained by assuming that streamwise drop velocities after primary breakup are roughly the same as streamwise velocities near the liquid surface. In particular, LHF computations of flow properties show that mean velocities in the liquid evolve from distributions appropriate for fully-developed pipe flow to a nearly flat profile having a velocity roughly $0.92\,\bar{u}_o$ in the region x/d < 20, relatively independent of specific flow conditions for the high Reynolds numbers used in these tests.[9,11] Thus, the lower streamwise drop velocities near the jet exit are due to the retarding effects of the jet passage walls on streamwise velocities near the liquid surface in this region.

In a similar manner, crosstream drop velocities appear to be comparable to crosstream velocity fluctuations in the liquid from the results illustrated in Fig. 3. In particular, $\tilde{v}_p/\bar{u}_o \approx 0.07$ for x/d < 20 with a tendency to decrease at larger values of x/d although this trend is not very clear due to scatter of the data. These values of $\tilde{v}_p/\bar{u}_o$ are compatible with velocity fluctuations for fully developed turbulent pipe flow (for turbulent pipe flow, maximum values of $\bar{v}'/\bar{u}_o$ and $\bar{u}'/\bar{u}_o$ are 0.05 and 0.10 from Refs. 13 and 14) and the rapid adjustment of velocity fluctuations near the surface of the liquid to the absence of the passage wall found from LHF computations.[9,11] These same calculations indicate that turbulence levels in the liquid decay proportional to $(x/d)^{-1/2}$ for x/d > 20 which may account for the tendency for $\tilde{v}_p/\bar{u}_o$ to decrease in this region. Taken together, the velocities of drops after turbulent primary breakup are typical of velocities in the liquid. This is not surprising due to the relatively large velocity relaxation times of the large drops that dominate the properties of mass averaged drop velocities.[10]

Onset of Breakup

The properties of the onset of turbulent primary breakup will be considered next because they provide valuable clues about the turbulent primary breakup mechanism. Properties of interest include conditions for turbulent primary breakup to occur at all, the drop sizes formed at the onset of breakup and the distance from the jet exit where breakup begins. The problem will be addressed by extending the preliminary considerations of Ruff et al.,[10] where the onset to breakup was associated with conditions where the momentum of turbulent fluctuations in the liquid was sufficient to overcome surface tension forces so that drops could be formed.

Some of the properties of the onset of turbulent primary breakup are illustrated in Fig. 4. These results involve measurements for water with d = 6.4 mm, showing the variation of drop sizes and the distance from the jet exit where breakup begins, SMD_i and x_i, as a function of the mean jet exit velocity. Correlations of these properties are shown along with the measurements; the development of the correlations will be discussed later.

The behavior of the onset of turbulent primary breakup illustrated in Fig, 4 is qualitatively similar to second wind-induced breakup of nonturbulent liquid jets.[4,5,14,15] This involves breakup along the sides of the liquid jet, rather than the liquid column as a whole, with the point where breakup begins moving toward the jet exit as the jet exit velocity increases. The same behavior can be seen in Fig. 4 for turbulent primary breakup, with breakup beginning very close to the jet exit (approximating the atomization breakup regime) at the highest velocities. Another feature of the results is that the SMD of the drops at the onset of turbulent primary breakup becomes smaller as the point of initial breakup moves toward the jet exit. Thus, the initiation of breakup is associated with conditions where the smallest drops can be formed. This trend also is supported by the photographs of Fig. 1, where drop sizes after primary breakup progressively increase with increasing distance from the jet exit.

Approximate analysis to find properties at the onset of turbulent primary breakup will be based on the configuration illustrated in Fig. 5. This involves the formation of a drop from a turbulent eddy having a characteristic size ℓ, and a characteristic crosstream velocity relative to the surrounding liquid v_ℓ. The eddy is shown with an elongated shape because length scales in the streamwise direction are larger than in the crossgeam direction for fully-developed turbulent pipe flow.[13,14] The eddy is assumed to be convected in the streamwise direction by the local mean velocity, which is taken to be $\bar{u}_o$ based on the results discussed in connection with Fig. 3. The drop formed by the eddy also is assumed to have a diameter comparable to ℓ.

Based on present measurements (e.g., Figs. 1 and 4), as well as time scale considerations to be considered subsequently, the drops at the onset of turbulent primary breakup are the smallest drops that can be formed by this mechanism. The smallest drop that can be formed is either comparable to the smallest scale of the turbulence, the Kolmogorov microscale, or the smallest eddy that has sufficient kinetic energy relative to its immediate surroundings to provide the surface energy needed to form a drop — whichever is larger. For fully-developed turbulent flow, the Kolmogorov length scale can be estimated as follows:[18]

$$\ell_k = 4\Lambda/(4\Lambda\,\bar{u}_o'/\nu_f)^{3/4} \quad (1)$$

where the streamwise integral length scale has been taken to be 4Λ, based on Laufer's measurements for fully-developed turbulent pipe flow.[14] For present test conditions, ℓ_k is in the range 1-10 μm, which is much smaller than the smallest drop size estimated from energy considerations, or observed experimentally, thus, only the latter requirement is relevant for present results.

The second criterion for the smallest drop that can be formed can be found by equating the kinetic energy of an eddy of characteristic size ℓ_i, relative to its surroundings, to the surface energy required to form a drop. This implies

$$\pi\,\rho_f \ell_i^3 v_{\ell_i}^2/12 \sim \pi\,\ell_i^2\sigma \quad (2)$$

where only proportionality is implied to account for effects of ellipticity, nonuniform velocities within the eddy and the efficiency of conversion of kinetic energy into surface energy. In order for drops to be formed at all, ℓ_i must be less than the largest eddies present, which is comparable to Λ,[10] while $\ell_k < \ell_i$ by definition for ***this*** primary breakup mechanism. Thus, it is reasonable to assume that ℓ_i is within the inertial range of the turbulence spectrum where ℓ_i and v_{ℓ_i} are related as follows:[18]

$$v_{\ell_i} \sim \bar{v}_o'\,(\ell_i/\Lambda)^{1/3} \quad (3)$$

where variations of turbulence properties within the liquid have been ignored. Combining Eqs. **(2)** and (3), setting $SMD_i = P_i$, and assuming that turbulence properties in the liquid can be approximated by jet exit turbulence properties, the following equation is obtained for the **SMD** at the onset of breakup:

$$SMD_i/\Lambda = C_{si}(\bar{u}_o/\bar{v}_o')^{6/5} We_{f\Lambda}^{-3/5} \quad (4)$$

where C_{si} is an empirical constant involving the various proportionality constants. With fully-developed turbulent pipe flow at the jet exit, $\bar{v}_o'/\bar{u}_o$ also is essentially constant,[13,14] so that SMD_i/Λ should only be a function of $We_{f\Lambda}$ for present test conditions.

Present measurements of SMD_i are plotted in terms of the variables of Eq. (4) in Fig. 6. The correlation of the data for all three liquids and jet diameters generally is within the scatter anticipated based on experimental uncertainties. The power of $We_{f\Lambda}$ for the correlation of the data is not -3/5 as suggested by Eq. (4), however, and can be represented better by the following empirical fit which is shown on the plot:

$$SMD_i/\Lambda = 133\,We_{f\Lambda}^{-0.74} \quad (5)$$

The standard deviations of the coefficient and power in Eq. (5) are 10 and 7%, respectively, and correlation coefficient of the fit **is 0.97.** The reduction of the power of $We_{f\Lambda}$ from -3/5 in Eq. **(4)** to -0.74 in Eq. (5) is statistically significant but is not large in view of the approximations used to develop the correlating expression and experimental uncertainties. The coefficient of Eq. *(5)* is relatively large but ***this*** can be anticipated from Eq. (4) if C_{si} is on the order of unity because $(\bar{u}_o/\bar{v}_o')^{6/5}$ is large for fully-developed turbulent pipe flow. Finally, SMD_i estimates from Eq. (5) are seen to be in excellent agreement with the measurements for water illustrated in Fig. 4.

The next step is to develop an expression for the distance from the jet exit, xi, where turbulent primary breakup is initiated. To find x_i, it is assumed that the drop-forming eddy convects along the liquid surface with a streamwise velocity $\bar{u}_o$, based on the results of Fig. **3.** Then the location of the onset of turbulent primary breakup becomes:

$$x_i = \bar{u}_o\,\tau_i \quad (6)$$

where τ_i is the time required for an eddy having a characteristic size, Pi, to form a drop. There are several characteristic times that can be associated with the time to form a drop. First of all, the protrusion of ligaments and their division into drops, seen in Figs. 1 and **2,** suggests use of the characteristic time for Rayleigh breakup. A second possibility is the characteristic time of the eddy, $\tau_i = \ell_i/v_{\ell_i}$, assuming that loss of the correlation of velocities near the surface causes the protruding ligament to become thin near its base and rapidly separate by Rayleigh breakup. **A** thud possibility involves aerodynamic secondary breakup of the protruding ligament discussed by Tseng et al.[12] Breakup times for this mechanism have not been established. However, secondary breakup times are relatively independent of the mode of breakup so that the correlation of Ranger and Nicholls[19] provides a reasonable estimate: this implies $\tau_i = \ell_i(\rho_f/\rho_g)^{1/2}/\bar{u}_o$ if the velocity of the gas near the liquid surface is assumed to be small. Unfortunately, breakup times of all three mechanisms are of the same order of magnitude for present test conditions so that the choice among them is not obvious. However, the time for Rayleigh breakup clearly is shortest near the jet exit, where onset of breakup occurs, and is supported by the appearance of the flow; therefore, this breakup time will be used in the following.

Considering Rayleigh breakup, ℓ_i is taken to be the diameter of a protruding ligament, having a jetting velocity of v_{ℓ_i}, from which the **first** drops **are** formed. Weber,[20] finds that breakup length, L_i, of liquid column can be expressed as follows:

$$L_i/\ell_i \sim (\rho_f \ell_i v_{\ell_i}^2/\sigma)^{1/2} + 3\,\mu_f v_{\ell_i}/\sigma \quad (7)$$

For present conditions, the second term in Eq. (7) is small and will be ignored in the following, although it could be **a** factor for very viscous liquids. Then assuming that τ_i is proportional to the time required for a ligament to grow to its breakup length, L_i/v_{ℓ_i}, τ_i becomes:

$$\tau_i \sim (\rho_f \ell_i^3/\sigma)^{1/2} \quad (8)$$

which is independent of v_{ℓ_i}. An expression for x_i **is** then found by substituting Eq. (8) into Eq. (6) and letting $SMD_i = P_i$ as before:

$$x_i/\Lambda \sim (SMD_i/\Lambda)^{3/2} We_{f\Lambda}^{1/2} \quad (9)$$

The results of Eq. (9) indicate that drop sizes increase with increasing distances from the jet exit, supporting the idea that the onset of turbulent primary breakup involves the smallest drops that can be formed. Finally, eliminating SMD_i from Eq. (9), using Eq. (4), the following correlating expression for x_i is obtained:

$$x_i/\Lambda = C_{xi} (\bar{u}_o/\bar{v}_o')^{9/5} We_{f\Lambda}^{-0.4} \quad (10)$$

where C_{xi} is a constant of proportionality and $(\bar{v}_o/\bar{u}_o)$ is a constant for fully-developed turbulent pipe flow at the jet exit.

Present measurements of x_i are plotted in terms of the variables of Eq. (10) in Fig. 7. The correlation of the data for all three liquids and jet diameters is reasonably good in view of the relatively large experimental uncertainties of x_i, similar to the correlation of SMD_i in Fig. 6. As before, however, the power of $We_{f\Lambda}$ for the correlation of the data is not -0.4 as suggested by Eq. (10) but can be represented better by the following empirical fit which is shown on the plot:

$$x_i/\Lambda = 3980\, We_{f\Lambda}^{-0.67} \quad (11)$$

The standard deviations of the coefficient and power in Eq. (11) are 10 and 128, respectively, and the Correlation coefficient of the fit is 0.91. The large value of the coefficient of Eq. (11) can be anticipated from Eq. (10), if C_{xi} is on the order of unity, because $(\bar{u}_o/\bar{v}_o')^{9/5}$ is quite large for turbulent pipe flow. Finally, x_i estimates from Eq. (11) are seen to be in excellent agreement with the measurements for water illustrated in Fig. 4.

A check of the internal consistency of the correlations for SMD_i and x_i is useful for developing an expression for the variation of SMD with distance from the injector. This can be done by combining the phenomenological expressions of Eqs. (4) and (10) to obtain an expression directly relating x_i and SMD_i, similar to Eq. (9), as follows:

$$x_i/\Lambda = (C_{xi}/C_{si}^{3/2})(SMD_i/\Lambda)^{3/2} We_{f\Lambda}^{1/2} \quad (12)$$

The coefficient of this expression is independent of $\bar{v}_o'/\bar{u}_o$ and is expected to have a value on the order of unity. Repeating the same exercise using the best fit correlations of Eqs. (5) and (11) yields:

$$x_i/\Lambda = 1.43[(SMD_i/\Lambda)^{3/2} We_{f\Lambda}^{1/2}]^{1.08} \quad (13)$$

Equation (13) is seen to be consistent with Eq. (12): the coefficient is on the order of unity and the power on the right-hand-side of Eq. (13) is not statistically different from unity in view of the standard deviations of the powers in Eqs. (5) and (11) — both as anticipated.

Drop Sizes and Shapes

Drop Sizes. The approach used to find an expression for the variation of SMD with distance from the jet exit was similar to the method used to find x_i. First of all, it is reasonable to assume that drops near the liquid surface have been recently formed because they have relatively large radial velocities (see Fig. 3). Additionally, the SMD is dominated by the largest drops in the drop size distribution; therefore, it also is plausible that the SMD is proportional to the largest drop that can be formed at a particular position, i.e., in the time available for the flow along the liquid surface to reach the position in question. Then, adopting the Rayleigh breakup mechanism and letting $SMD = \Lambda$, as before, a procedure similar to the derivation of Eq. (9) yields the following expression for the variation of SMD with distance from the jet exit:

$$SMD/\Lambda = C_{sx} [x/(\Lambda\, We_{f\Lambda}^{1/2})]^{Y3} \quad (14)$$

where C_{sx} is a constant of proportionality that should be on the order of unity.

Under present assumptions, the principles relating SMD to x are the same for both the onset of breakup and at larger distances from the jet exit. Thus, comparing Eqs. (13) and (14) suggests that SMD/Λ should be correlated as a function of $x/(\Lambda\, We_{f\Lambda}^{0.54})$ for consistency. Available measurements from the present study, including onset of breakup conditions, as well as Refs. 9, 10 and 12 at atmospheric pressure, are plotted in this manner in Fig. 8. Two correlations of the data are shown on the plot as well: the best fit of all the data and Eq. (13) for onset of breakup conditions alone. The best fit correlation of all the data is:

$$SMD/\Lambda = 0.69[x/(\Lambda\, We_{f\Lambda}^{0.54})]^{0.57} \quad (15)$$

The standard deviations of the coefficient and power of Eq. (15) are 14 and 3%, respectively, and the correlation coefficient of the fit is 0.98.

Differences between the two correlations illustrated in Fig. 8 are small in comparison to experimental uncertainties so that drop formation both at the onset of breakup and at distances farther from the jet exit appears to be similar. The SMD of the smallest drops, formed at the onset of breakup, are in the range 10-20 μm which is roughly an order of magnitude larger than the Kolmogorov length scales for these test conditions. The characteristics of turbulent primary breakup should change when breakup involves Kolmogorov-sized drops which is an interesting issue for future study. The largest SMD observed in the data base illustrated in Fig. 8 approaches the order of magnitude of the radial integral scales of the turbulence. Somewhat larger scale drops are feasible because one-dimensional turbulence spectra still have significant energy at scales somewhat larger than the radial integral scale.[18] However, much larger SMD than those shown in Fig. 8 are unlikely for found liquid jets because of the finite length of the liquid core. This is indicated in Fig. 8 using the correlation for liquid core length (or jet breakup length) from Grant and Middleman:[4]

$$L_c/d = 8.51\, We_{fd}^{0.32} \quad (16)$$

where the range of L_c/d shown in the figure results from the variation of We, over the present test range. A more recent correlation of liquid core length for atomization breakup conditions, due to Chehroudi et al.,[7] yields core length limitations similar to those pictured in Fig. 8 but the range of L_c/d is somewhat broader because it does not involve We_{fd} explicitly. The fact that the SMD approaches A near the end of the liquid core, and thus is comparable to the diameter of the liquid core itself, is consistent with the liquid column breaking up as a whole in this region.

Ellipticity. Measurements of volume averaged ellipticity are plotted as a function of x/d in Fig. 9. The data shown include present measurements, which includes onset of breakup conditions, as well as the measurements of Refs. 9, 10 and 12 at atmospheric pressure. The measurements exhibit significant scatter, particularly at large x/d, and no correlation in terms of x/d should be implied by the plot. Nevertheless, the results help to complete the physical picture of the flow.

The measurements of e_p in Fig. 9 have values near unity at low x/d, which then increase toward a value of roughly 2 for x/d on the order of 100. This trend can be explained from the properties of both the turbulence spectrum and Rayleigh breakup, in connection with the observations of SMD/Λ illustrated in Fig. 8. For small values of x/d, SMD/Λ is quite small so the drops are formed from eddies at the high wave number end of the turbulence spectrum, approaching Kolmogorov length scales. Eddies in this region are nearly isotropic so that the drops formed by primary breakup are expected to be nearly round as well. In addition, conditions at small x/d appear to be dominated by Rayleigh breakup of ligaments protruding from the surface as discussed in connection with Fig. 1. Rayleigh breakup generally yields round drops rather quickly after breakup is completed when the diameter of the liquid column is small, which is typical of conditions near the jet exit.[20]

In contrast to the near jet exit region, several factors suggest increasing e_p after primary breakup as x/d increases. First of all, drop sizes after primary breakup progressively increase with x/d so that the time required for a detached drop to evolve to a round drop from the elongated shape immediately upon Rayleigh breakup increases which increases the probability of observing drops having large e_p. In particular, Rayleigh breakup theory implies a length-to-diameter of a drop at the instant of breakup of roughly 4:1,[20] which is comparable to the maximum values of e_p seen in Fig. 9. Another factor is that SMD/Λ approaches unity at large x/d so that drops are formed from eddies at the low wave number portion of the turbulence spectrum in this region. Integral-scale sized eddies exhibit anisotropy characteristic of the ratio of streamwise to crosstream spatial integral scales, which also is 4:1 for fully-developed pipe flow (assuming that liquid turbulence is similar to jet exit conditions).[14] Thus, drops formed by primary breakup at large x/d might be expected to have e_p of similar magnitude which is consistent with the observations of Fig. 9, as well.

Discussion

The present results suggest that most features of turbulent primary breakup observed at atmospheric pressure — conditions at the onset of breakup and the variation of SMD and e_p with distance after breakup begins — can be explained by interactions between liquid turbulence and Rayleigh breakup of ligaments protruding from the surface, ignoring aerodynamic effects. Observations during a companion study by Tseng et al.[12] of effects of ambient density on the properties of pressure-atomized sprays near the jet exit, however, show that aerodynamic effects also can be a factor in turbulent primary breakup. This involves a tendency for primary and secondary breakup to merge as the density of the ambient gas increases. It is argued in Ref. 12 that the onset of aerodynamic effects begins at air densities somewhat greater than atmospheric pressure conditions, however, definitive evidence that present results have not been influenced by aerodynamic effects currently is not available. Thus, present findings should be treated as provisional until the issue of the importance of aerodynamic effects is resolved. Work with this objective in mind has been initiated in this laboratory.

Conclusions

Primary breakup within the multiphase mixing layer of the near jet-exit region of large-scale pressure-atomized sprays was studied, considering liquid jets in air at atmospheric pressure with fully-developed turbulent pipe flow at the jet exit. The major conclusions of the study are as follows:

1. Drop size distributions after turbulent primary breakup approximate Simmons' universal root normal distribution with MMD/SMD = 1.2, similar to drops after nonturbulent primary breakup and at local conditions within the multiphase mixing layer of sprays.[1,9,10,12] Thus, the entire drop size distribution can be characterized by a single parameter like the SMD.

2. Mass-averaged mean drop velocities after turbulent primary breakup approximate mean and rms velocity fluctuations of the liquid in the streamwise and crosstream directions, respectively (cf. Fig. 3).

3. Drop sizes at the onset of turbulent primary breakup could be explained by equating the surface tension energy required to form a drop to the kinetic energy of a corresponding liquid eddy relative to its surroundings within the inertial region of the turbulence spectrum. This indicates a close correspondence between liquid turbulence properties and turbulent primary breakup (cf. Fig. 6).

4. The onset of turbulent primary breakup always occurred at some distance from the jet exit but approaches the exit, approximating atomization breakup conditions, at large $We_{f\Lambda}$. The distance required for the onset of breakup could be explained considering the residence time needed to initiate Rayleigh breakup of ligaments protruding from the liquid surface (cf. Fig. 7).

5. Drop sizes from turbulent primary breakup increased with distance from the jet exit, with the SMD reaching values on the order of the radial spatial integral scale of the liquid turbulence as the end of the liquid core is approached. Additionally, the effect of streamwise distance on SMD was virtually the same at the onset o breakup and thereafter. This behavior could be explained by associating the SMD with the largest drops that had sufficient residence time in the flow to be formed at the point in question by Rayleigh breakup of protruding ligaments (cf. Fig. 8).

Present results are limited to liquids having moderate viscosities at conditions where the SMD at the onset of breakup is at least an order of magnitude greater than the Kolmogorov length scale of the liquid turbulence. Consideration of the Rayleigh breakup mechanism of ligaments protruding from the surface suggests potential effects of liquid viscosities on breakup times, and limitations of the breakup mechanism as Kolmogorov length scales are approached, that should be explored. Additionally, limited data on turbulent primary breakup at

various ambient gas densities from Ref. 12 suggests potential aerodynamic effects at pressures greater than atmospheric pressure. Until these effects are resolved, it is not recommended to apply the correlations reported here beyond the present test range.

Acknowledgements

This research was sponsored by the Office of Naval Research Grant No. N00014-89-J-1199 under the technical management of G. D. Roy. Initial development of instrumentation was sponsored by the Air Force Office of Scientific Research, Grant No. 89-0516 with J. M. Tishkoff serving as technical manager. The U.S. Government is authorized to reproduce and distribute copies for governmental purposes notwithstanding any copyright notation thereon.

References

[1]Wu, P.-K., Ruff, G.A. and Faeth, G.M., "Primary Breakup in Liquid/Gas Mixing Layers," ***Atomization and Sprays,*** in press.

[2]De Juhasz, K.J., Zahm, O.F.. Jr. and Schweitzer, P.H., "On the Formation and Dispersion of Oil Sprays," Bulletin No. 40, Engineering Experimental Station, Pennsylvania State University, University Park, PA, 1932, pp. 63-68.

[3]Lee, D.W. and Spencer, R.C., "Photomicrographic Studies of Fuel Sprays," NACA Report No. 454, 1933.

[4]Grant, R.P. and Middleman, S., "Newtonian Jet Stability," *AIChE J.*, Vol. 12, July 1966, pp. 669-678.

[5]Phinney, R.E., "The Breakup of a Turbulent Jet in a Gaseous Atmosphere," ***J. Fluid Mech.,*** Vol. 88, 1977, pp. 119-127.

[6]Hiroyasu, H., Shimizu, M., and Arai, M., "The Breakup of a High Speed Jet in a High Pressure Gaseous Environment," Univ. of Wisconsin, Madison, ICLASS-82, 1982.

[7]Chehroudi, B., Onuma, Y., Chen, S.-H. and Bracco, F. V., "On the Intact Core of Full Cone Sprays," ***SAE*** Paper No. 850126, 1985.

[8]Ruff, G.A., Sagar, A.D. and Faeth, G.M., "Structure of the Near-Injector Region of Pressure-Atomized Sprays," *AIAA J.*, Vol. 27, July 1989, pp. 549-559.

[9]Ruff, G.A., Bernal, L.P. and Faeth, G.M., "Structure of the Near-Injector Region of Non-Evaporating Pressure-Atomized Sprays," ***J. Prop. Power,*** Vol. 7, Mar.-April, 1991, pp. 221-230.

[10]Ruff, G.A., Wu, P.-K., Bernal, L.P., and Faeth, G.M., "Continuous- and Dispersed-Phase Structure of Dense Nonevaporating Pressure-Atomized Sprays," ***J. Prop. Power,*** in press.

[11]Tseng, L.-K., Ruff, G.A. and Faeth, G.M., "Effects of Gas Density on the Structure of Liquid Jets in Still Gases," *AIAA J.*, in press.

[12]Tseng, L.-K., Wu, P.-K. and Faeth, G.M., "Dispersed-Phase Structure of Pressure-Atomized Sprays at Various Gas Densities," AIAA Paper No. 92-0230, 1992.

[13]Schlichting, H., ***Boundary Layer Theory,*** 7th ed., McGraw-Hill, New York, 1979, p. 599.

[14]Hinze, J.O., ***Turbulence,*** 2nd ed., McGraw-Hill, New York, 1975, pp. 427 and 724-742.

[15]Miesse, C.C., "Correlation of Experimental Data on the Disintegration of Liquid Jets," *Ind. Engr. Chem.*, Vol. 47, 1955, pp. 1690-1697.

[16]Ranz, W.E., "Some Experiments on Orifice Sprays," ***Can. J. Chem. Engr.,*** Vol. 36, 1958, pp. 175-181.

[17]Simmons, H.C., "The Correlation of Drop-Size Distributions in Fuel Nozzle Sprays," ***J. Engr. for Power*** , Vol. 99, July 1977, pp. 309-319.

[18]Tennekes, H. and Lumley, J.L., ***A First Course in Turbulence,*** M.I.T. Press, Cambridge, MA, 1972, pp. 248-286.

[19]Ranger, A.A. and Nicholls, J.A., "Aerodynamic Shattering of Liquid Drops," *AIAA J.*, Vol. 7, February 1969, pp. 285-290.

[20]Weber, C., "Zum Zerfall eines Flussigkeitsstrahles," *Z. Angew. Math. Mech.,* Vol. 2, 1931, pp. 136-141.

Table 1 Summary of Test Conditions[a]

Liquid	Water	Glycerol (42%)	n-Heptane
ρ_f (kg/m^3)	997	1101	683
$\mu_f \times 10^4$ (kg/ms)	8.94	34.66	3.94
$\sigma \times 10^2$ (N/m)	7.08	6.30	2.00
d (mm)	3.6,6.4, 9.5	6.4	6.4
$\bar{u}_o$ (m/s)	16-109	32-99	20-45
$Re_{fd} \times 10^{-4}$	11-78	6-20	22-50
We_{gd}	27-1257	122-1160	154-778
$We_{fd} \times 10^{-4}$	2.3-106	11.4-109	8.7-44
$Oh_d \times 10^3$	1.09-1.77	5.23	1.10

[a]Pressure-atomized injection vertically downward in still air at 98.8 kPa and 298 ± 3 K with fully-developed turbulent pipe flow at the jet exit (injector passage length/diameter ratio of 41).
[b]Data for water ford = 9.5 mm obtained from Ruff et al.[9,10] and Tseng et al.[12]

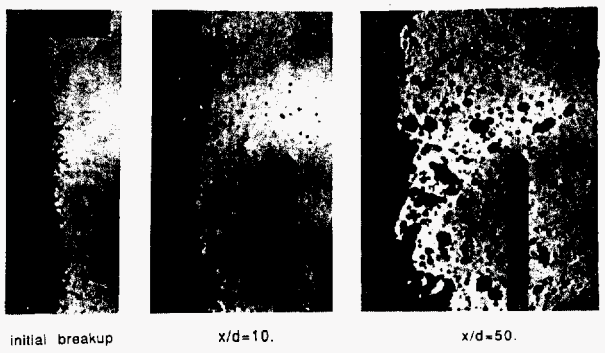

Fig. 1 Pulsed shadowgraphs of the flow near the liquid surface at various distances from the jet exit.

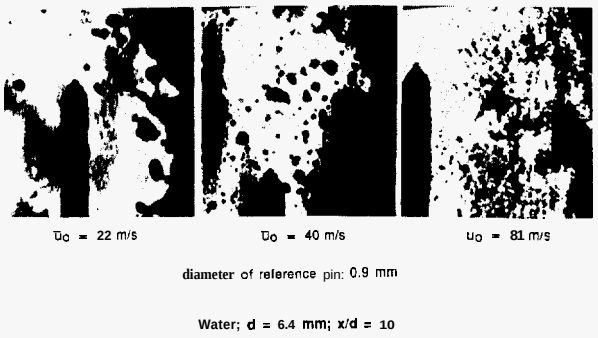

Fig. 2 Hologram reconstructions of flow near the liquid surface at various relative velocities.

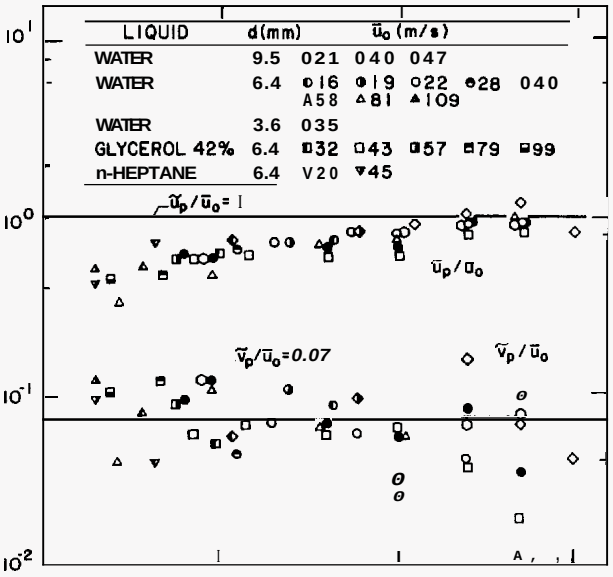

Fig. 3 Mass averaged drop velocities after primary breakup as a function of distance from the jet exit.

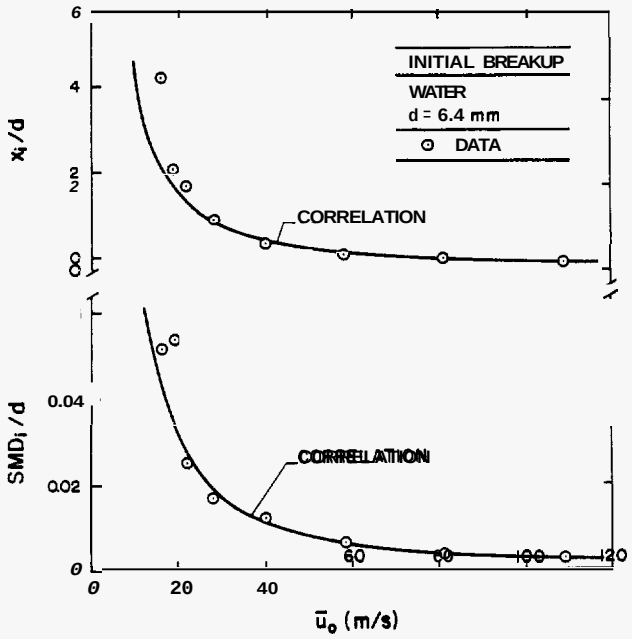

Fig. 4 Initial breakup position and SMD as a function of jet exit velocity: water, d = 6.4 mm.

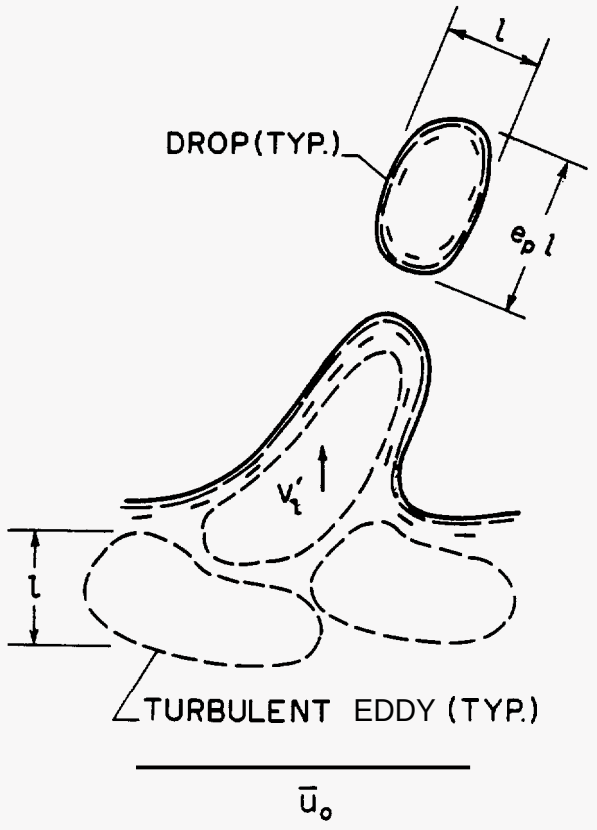

Fig. 5 Sketch of turbulent primary breakup at the liquid surface.

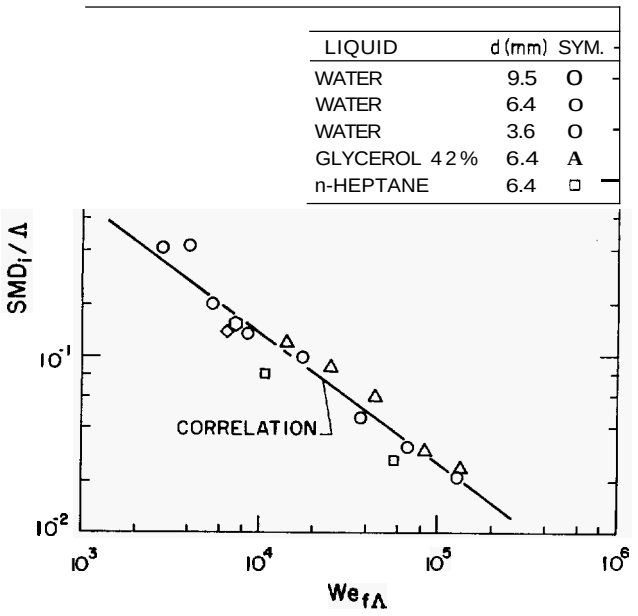

Fig. *6* SMD at initiation of turbulent primary breakup as a function of $We_{f\Lambda}$.

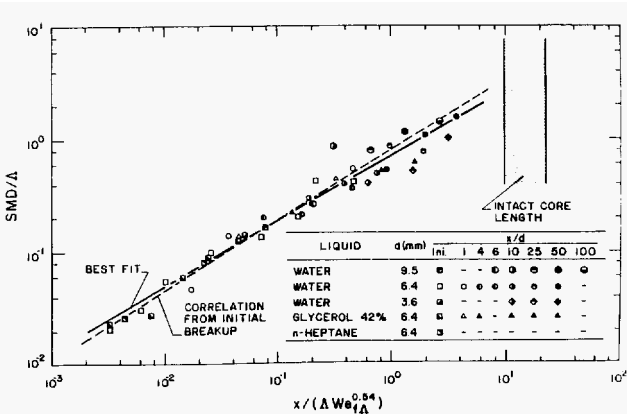

Fig. 8 SMD after turbulent primary breakup as a function of distance from the jet exit.

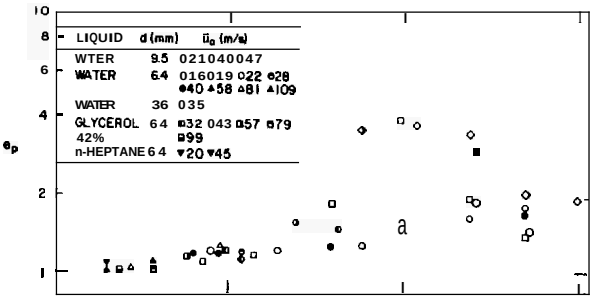

Fig. 9 Ellipticity after turbulent primary breakup as a function of distance from the jet exit.

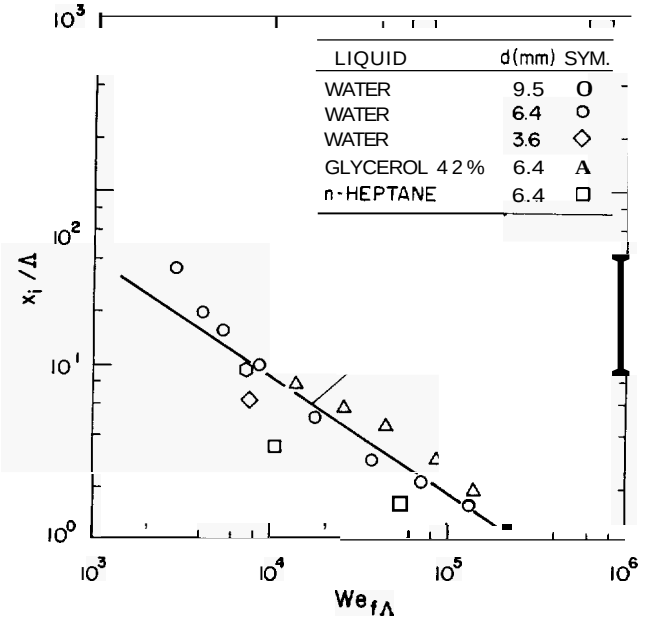

Fig. 7 Length to initiate turbulent primary breakup as a function of $We_{f\Lambda}$.